Vol. 569: 77–88, 2017
https://doi.org/10.3354/meps12088

MARINE ECOLOGY PROGRESS SERIES
Mar Ecol Prog Ser

Published April 7

FTIR imaging analysis of cell content in sea-ice diatom taxa during a spring bloom in the lower Northwest Passage of the Canadian Arctic

Nicole M. Pogorzelec[1], C. J. Mundy[1,*], Catherine R. Findlay[2], Karley Campbell[1], Aura Diaz[1], Jens K. Ehn[1], Søren Rysgaard[1], Kathleen M. Gough[2,*]

[1]Centre for Earth Observation Science (CEOS), and [2]Department of Chemistry, University of Manitoba, Winnipeg, Manitoba R3T 2N2, Canada

ABSTRACT: During their vernal bloom, ice algae respond to variable light and nutrient availability by changing their production of cellular lipids and proteins. Fourier transform infrared (FTIR) spectrochemical imaging was used to quantify relative amounts of saturated lipids and proteins within algal cells from high and low light conditions, i.e. thin and thick snow cover, respectively. Samples were collected within the lower Northwest Passage, near Cambridge Bay, Nunavut, Canada during the 2014 ICE-CAMPS field campaign. Diatom taxa analyzed included *Nitzschia frigida*, pennate ribbon colonies, and *Attheya* spp. Saturated lipid content and lipid to protein ratios were significantly greater under thin snow covers relative to those under thick; cell protein content remained relatively stable throughout the study under both snow covers. Results have been interpreted relative to a concurrent, related study wherein under-ice nutrients were concluded to be limited throughout the study. Taxa responses reported herein differed according to size, with *N. frigida* exhibiting the earliest and most dramatic changes. The increase in lipid to protein ratio highlighted the transitioning allocation of carbon from protein to lipid algal biomass through the spring bloom progression, with increasing light under nutrient limiting conditions in this location.

KEY WORDS: Arctic diatom · FTIR · Sea-ice algae · Light and nutrient limitation · Biomass composition · Proteins · Saturated lipids

INTRODUCTION

Ice algal communities, dominated by diatoms, thrive at the bottommost sea ice layer in the Arctic (Różańska et al. 2009, Poulin et al. 2011), where they serve as the primary pulse of photosynthetic production during the spring bloom (Legendre et al. 1992, Leu et al. 2015). Essential lipids and fatty acids (saturated and poly-unsaturated) are produced during the ice algal bloom, providing nourishment to the energy-rich Arctic food web (Smith et al. 1987, Mock & Gradinger 2000, Leu et al. 2010). Due to rising global temperatures, the later freeze-up and earlier melt onset (Markus et al. 2009, Stroeve et al. 2012, Parkinson & Comiso 2013) will likely have a strong influence on the ice algal community and its bloom period. A later freeze-up can decrease ice algal colonization due to a reduction in water column algal standing stock from fall to winter transitions (Niemi et al. 2011). Earlier melt can accelerate termination of the ice algal bloom (Fortier et al. 2002, Mundy et al. 2005), creating mismatched trophic cascades (Søreide et al. 2010, Leu et al. 2011) that can affect the Arctic marine food-web structure.

*Corresponding authors: cj.mundy@umanitoba.ca, kathleen.gough@umanitoba.ca

With their unique silica-based frustule, the relatively fast biomass-based growth rate of diatoms leads to their common dominance in algal blooms that form in nutrient-replete environments (Lalli & Parsons 1997, Miller & Wheeler 2012). Pennate diatoms typically dominate the Arctic ice algal community (Różańska et al. 2009, Poulin et al. 2011). Ice algal growth is generally light-limited during early spring (Gosselin et al. 1990, Leu et al. 2015), as a result of low seasonal insolation intensity, along with the high attenuation of snow-covered sea ice (Perovich et al. 1998). Net photosynthetic rates are lowered under heavily shaded light conditions, resulting in a reduction in cellular inorganic carbon assimilation, and thus, less accumulation of algal biomass (Mock & Gradinger 2000, Mock & Kroon 2002a). As the solar angle increases, the amount of photosynthetically active radiation (PAR) reaching the ice algal community increases. Due to the variable snow cover, ice algae must acclimate to compensate for rapid changes in their environment (Kirst & Wiencke 1995, Leu et al. 2010). When conditions are favourable (e.g. under thinner snow cover and greater light), algal cells acclimate by decreasing their chloroplast count per cell (Gosselin et al. 1990, Kirst & Wiencke 1995), which decreases the protein-rich photosystem II reaction centres, as well as other structural proteins (Campbell et al. 2008, Gosselin et al. 1990). Towards the later stage of the spring bloom, ice algae can rapidly exhaust their nutrient supply (Leu et al. 2015). This nutrient-limiting condition will also result in allocation of carbon to storage and structural lipids (Smith et al. 1997, Mock & Kroon 2002a).

Here we report the first use of Fourier transform infrared (FTIR) spectrochemical imaging for quantification of intracellular biomass composition of individual diatoms. In contrast to other studies in which light and nutrient limitation responses were based on community (bulk) ice algal biomass composition (Cota & Smith 1991, Mock & Kroon 2002b, Leu et al. 2010), our assessment was performed on individual cells to yield taxa-specific biomolecular responses to light and nutrient limitation during the vernal bloom. Samples were collected during the Ice Covered Ecosystem-Cambridge Bay Process Study (ICE-CAMPS) 2014 campaign (March to May), in the lower Northwest Passage, Nunavut, Canada. Change in biomass composition over the Arctic vernal bloom was determined for individual diatom taxa: *Nitzschia frigida* (pennate), pennate ribbon colonies (mainly *Fragilariopsis* cf. *cylindrus*), and *Attheya* spp. (centric), under thick and thin snow cover.

MATERIALS AND METHODS

Field data collection

During the ICE-CAMPS 2014 field campaign, ice algal samples were collected from the bottom skeletal layer under snow-covered landfast first-year sea ice in Dease Strait (69° 1.62′ N, 105° 19.70′ W), near Cambridge Bay, Nunavut, Canada. Sampling occurred from 11 to 15 March, and from 21 April to 30 May 2014, under both thick (15 to 20 cm) and thin (3 to 12 cm) snow covers, with a sampling frequency of approximately 4 d. For each sample, 2 ice cores were collected using a 9 cm inner diameter Mark II Coring System (Kovacs Enterprises). Algal cells were acquired by scraping the bottom ~0.5 cm layer directly into an opaque, high-density polyethylene bottle containing at least 500 ml of cooled 0.2-µm filtered seawater, to limit osmotic stress associated with ice melt. The extracted ice cores were shielded from direct solar radiation during this step. After the ice melted, an aliquot was taken from a gently and thoroughly mixed sample and filtered onto a 5 µm pore, 25 mm diameter polycarbonate membrane filter (SterliTech), which was folded in half, wrapped in an aluminum casing and immediately stored at –80°C.

Daily averaged meteorological measurements were recorded between 10 and 31 May 2014. Air temperature was acquired from a HC2-S3 temperature probe (211 cm from the surface). Surface shortwave (300 to 3000 nm) albedo (both downwelling and upwelling radiation) was obtained with a CNR4 (Kipp & Zonen) net radiometer (110 cm from the surface) and recorded with a CR3000 data logger (Campbell Scientific). Top of the atmosphere (TOA) shortwave radiation was calculated based on latitude, with the 1367 W m^{-2} as the solar constant (NREL 2016).

Sample preparation

Diatom preparation and FTIR image collection followed the methodology described in Findlay et al. (2015). Briefly, 4 to 8 µl of MilliQ water was pipetted onto a 25 mm diameter, 2 mm thick BaF_2 IR substrate (Pike Technologies). A portion of a polycarbonate filter was applied to the water droplet to release diatoms. After the diatoms had settled to the window surface (<1 min), excess water was wicked off with lens tissue. The sample was viewed under a light microscope to determine diatom location and taxonomic classification; photo references of chosen targets were recorded at 4×, 10×, and 40× magnifica-

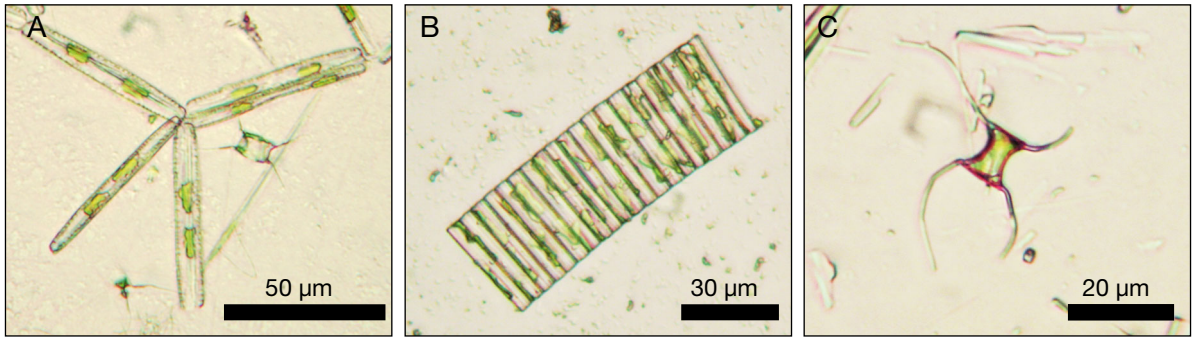

Fig. 1. Microscope images of 3 diatom taxa: (A) *Nitzschia frigida*, (B) pennate ribbon colony, and (C) *Attheya* spp.

tion. The loaded BaF_2 window was dried overnight in a dark desiccant chamber to minimize photo-oxidation of lipids (Stitt et al. 2012). At least 3 replicates of each target taxa were measured from samples at low and at high snow cover, per sample date.

Diatom selection

The number and variety of algal species captured on the filters varied considerably from March to May. Diatom taxa in this study were selected based on their observed dominance throughout the monitored bloom period. Typical examples of the taxa selected are shown in Fig. 1; they included 2 colony-forming pennate taxa, *Nitzschia frigida* (average cell size 60 × 8 µm) and a ribbon colony (average cell size 25 × 4 µm), as well as one centric diatom, *Attheya* spp. (average cell size 9 × 8 µm, not including setae). Several species of *Attheya* were identified in the ice algal community (K. Campbell unpubl. data). This genus dominated taxonomic composition during the latter half of the ice algal bloom, with the epiphytic and common sea ice algae (Poulin et al. 2011), *A. septentrionalis*, being one of the most abundant identified species (K. Campbell unpubl. data). All *Attheya* cells examined with FTIR were unattached, but the visible structure and morphology was identified as likely belonging to young cells of *A. septentrionalis* (S. Lessard pers. comm.). Similarly, clear species identification as *Fragilariopsis cylindrus* was possible for most, but not all, of the ribbon colonies; however, the remainder were very similar. Confirmation of *F. cylindrus* by electron microscopic examination of the frustule was not feasible and chloroplast structure was altered by the freeze, thaw and desiccation process. Accordingly, these 2 taxa are referred to as '*Attheya* spp.' and 'pennate ribbon colonies', respectively, herein. Where possible, a minimum of 3 and up to 18 diatom cells of each taxa were examined per collection day (see Table S1 in the Supplement at www.int-res.com/articles/suppl/m569p077_supp.pdf). No pennate ribbon colonies were analyzed under thin snow cover on 28 and 30 May as neither intact nor broken remnants could be found in the samples.

FTIR spectroscopy of diatoms

The target cells were imaged by FTIR in transmittance mode, within 24 to 48 h of preparation. Images were acquired with an Agilent Cary 670 FTIR spectrometer coupled to a 620 IR imaging microscope, equipped with 15×, 0.62 NA objective and condenser, and additional magnification optics directly in front of the 64 × 64 pixel focal plane array (FPA) detector. Final pixel dimensions in the FPA images were 1.1 × 1.1 μm^2 (Findlay et al. 2015). A complete FTIR spectrum is recorded at each pixel of the FPA and ratioed to a background spectrum recorded from a clean region of the BaF_2 window. All spectra were recorded at 4 cm^{-1} spectral resolution with a zero-fill factor of 2 (Findlay et al. 2015); 512 scans were co-added for the background and 256 for the diatoms.

Under IR light, each unique molecular compound within a target absorbs a specific set of IR energies that cause vibrational motions (stretch, bend, twist, etc.). A plot of absorbance intensity (Abs), calculated as (–log[transmittance]), versus wavenumber (cm^{-1}) constitutes an IR spectrum (Griffiths & de Haseth, 2007). IR spectra of diatoms give rise to a well-defined set of absorbance bands for which the functional group assignments are known (Stehfest et al. 2005, Sackett et al. 2013, 2016, Findlay et al. 2015).

The relative intensities in the spectra recorded in an FPA image depend on the composition at each location (pixel). Typical spectra from the frustule only and from a chloroplast seen through the frustule are shown in Fig. 2. The blank spectrum was taken from a point distant from the cell; some Si-O is evident,

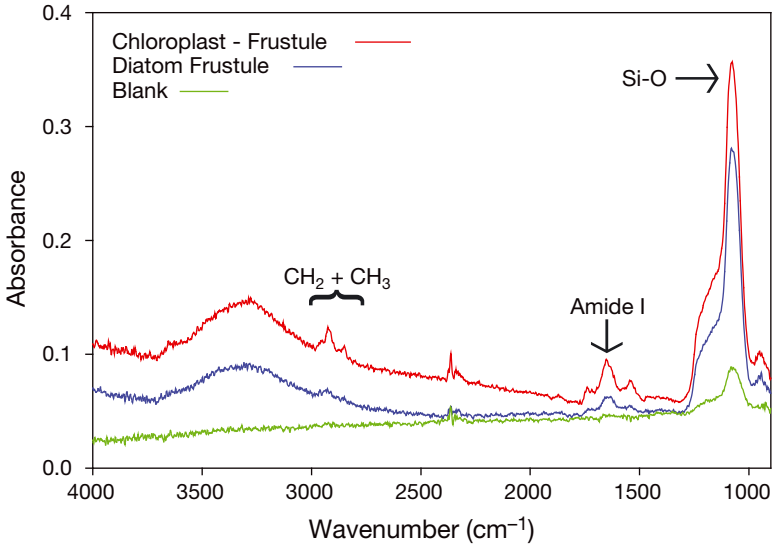

Fig. 2. Typical spectra from a Fourier transform infrared (FTIR) image of a single diatom cell, selected from the chloroplast seen through the frustule, the frustule alone, and a blank region beyond the cell. Absorbance bands due to biomass functional groups of interest are labeled: CH_2+CH_3 (lipid), Amide I (protein), and Si-O (silica)

presumably from dissolved salts in the sea ice. The chloroplast is much richer in protein (proxy: Amide I band at 1655 cm^{-1}) and hydrocarbon (CH_2+CH_3) than the frustule. Note that the profile of the CH-stretch region matches that of saturated lipid, with strong CH_2 bands at 2920 and 2850 cm^{-1} and less intense CH_3 bands at 2956 and 2873 cm^{-1}. Mono- and poly-unsaturated fatty acids have been reported to comprise the major fraction of the fatty acid complement in diatoms (Leu et al. 2010) but these often contain only 1 or 2 unsaturated C=C bonds per molecule. Hence, the actual number of unsaturated functional groups identified would have been at most 15% of the total hydrocarbon load in early spring, dropping to 10% towards the later stage of the bloom. Leu et al. (2010) attributed this decrease to photo-oxidation by increasing levels of UV light. The IR absorbance band for the C–H stretch of an unsaturated functional group (=C–H) occurs at 3010 cm^{-1}, but none was observed, even in spectra summed to represent an entire diatom. We attribute this absence to photo-oxidation of the samples (Stitt et al. 2012), despite efforts to minimize losses during handling. For simplicity, the CH-stretch region is referred to herein as saturated lipid.

FTIR spectrochemical image analysis

Relative quantities of major biomass components are represented by the relative intensities of their FTIR absorbance bands in the spectra at each pixel in the FPA image. The distribution of saturated lipid, protein, and silica were determined by integration of the relevant band areas (Resolutions Pro™, version 5.2.0, Agilent Technologies). The results were displayed as false-colour spectrochemical images to provide a rapid visual assessment of the distribution of the biomass components and to allow preliminary verification of data quality (see 'Results').

Saturated lipid (CH_2+CH_3) bands were integrated between 2969.84 and 2840.63 cm^{-1}, with baseline defined at 3004.55 and 2807.85 cm^{-1}. The Amide I (hereafter 'protein') band area was integrated between 1685.48 and 1610.27 cm^{-1}, with baseline defined at 1805.05 and 1488.78 cm^{-1}. The integration parameters for the silica band were 1093 to 1053 cm^{-1}, baseline set at 1113 and 1044 cm^{-1}. The complete FTIR image data files were exported into MATLAB™ so that individual diatoms could be computationally isolated and relative algal biomass content determined (in-house code; Findlay et al. 2017). In each case, a threshold was required to exclude pixels containing low silica content from seawater (shown in the 'blank' spectrum in Fig. 2, with a silica peak at 1075 cm^{-1}). The outline of the diatom was confirmed by comparing the visible image with the false color Si-O image. Single-celled species were immediately processed for the total saturated lipid and protein content, divided by the total number of outlined diatom pixels, to yield average content per cell. Where multiple diatom cells were detected in the field of view, cells were masked individually. Average relative values were calculated for saturated lipid and protein content per cell, as well as ratio of saturated lipid to protein, per cell.

Statistical analysis

Linear and exponential regression trends were calculated in Sigma Plot (version 12.5) for biomass composition: saturated lipid, protein, and ratio (saturated lipid to protein) versus time. A matched pairs, 1-tailed Student's *t*-test analysis was performed to determine the differences between thin and thick snow cover biomass (JMP 4 software).

RESULTS

Environmental conditions

Meteorological parameters were only recorded from 8 to 30 May (Fig. 3A–C). Prior to these dates, it was assumed that the surface shortwave albedo remained stable at a relatively high value; this assumption is supported by Environment Canada data from Cambridge Bay airport (69° 6.5′ N, 105° 8.3′ W; Environment Canada 2016). Daily averaged air temperatures (Fig. 3A) varied from a low of −8.7°C on 13 May to a high of 2.3°C on 29 May, with the temperatures surpassing 0°C on 28 May. The incident shortwave radiation increased gradually over time; values reached a maximum irradiance of 308 W m^{-2} on 24 May, but dropped to a minimum of 193 W m^{-2} on 25 May (Fig. 3B), owing to a substantial snowfall from a warm, low pressure system. The seasonal increase of irradiance over the entire study, reported as daily averaged shortwave radiation at the TOA for the latitude of our study site, increased from 115 W m^{-2} on 11 March to 462 W m^{-2} on 30 May (Fig. 3B). Surface shortwave albedo remained steady until 24 May, then decreased (Fig. 3C) with the onset of melt.

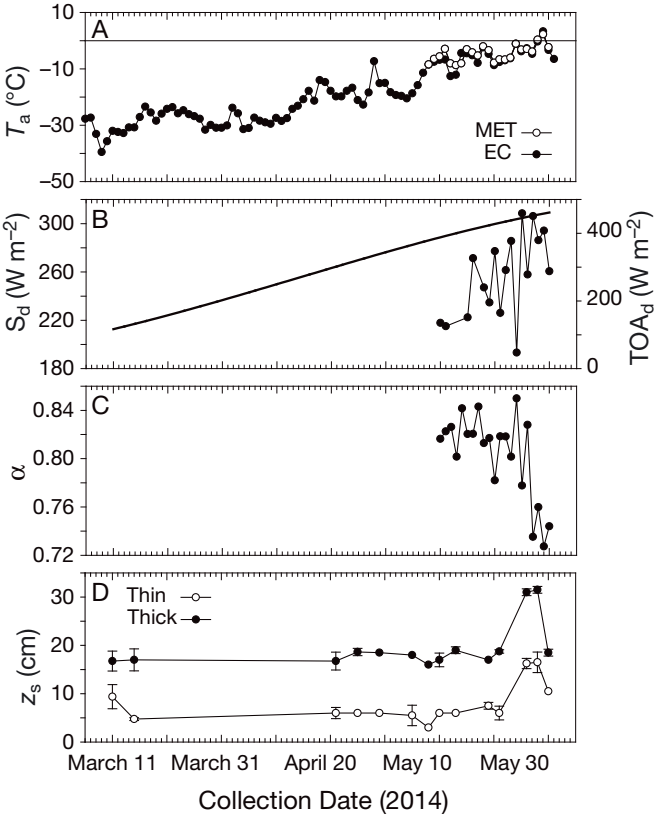

Fig. 3. Meteorological parameters: (A) daily averaged air temperature (T_a) recorded at the on-ice meteorological station (MET) and obtained through Environment Canada (EC); (B) downwelling shortwave irradiance at top of the atmosphere (TOA_d, solid line) and surface (S_d, line with data points); (C) shortwave albedo (α); (D) average snow depth (z_s) in areas of (○) thin and (●) thick snow cover

Stable snow drifts enabled consistent sampling of thick and thin snow cover sites for most of the study, with depths of 17.6 ± 1.0 cm and 5.9 ± 1.6 cm respectively (Fig. 3D), except for sites sampled after 26 May. Due to a snowstorm on 25 May, snow thickness increased evenly at the study site to an average value of 31.3 cm (thick) and 16.4 cm (thin) on 26 and 28 May. Snow re-distribution by wind re-exposed the original snowdrifts by the 30 May sample date.

FTIR spectrochemical imaging

The spectrochemical image analysis of a *Nitzschia frigida* colony is illustrated in Fig. 4. The spectrum in Fig. 4A was extracted from the biologically rich chloroplast region of the cell. The light microscope photo (Fig. 4B) provided a reference for the processed spectrochemical images; the pixel location for the selected IR spectrum is shown as a bolded **X**. The relative amount and distribution of the components across the cell were calculated as the integrated band intensity in the spectrum at each pixel in the image, and converted to false colour images for display. Here, as in all diatoms examined, saturated lipid and protein content were concentrated in the chloroplast region of the cell (Fig. 4C,D), while the silica content defined the extent of the individual diatom frustule (Fig. 4E). This field of view contained 3 complete cells; selective masking was performed in MATLAB™ to yield separate lipid and protein content values for each cell.

Saturated lipid

Matched pairs Student's *t*-tests showed that snow cover had a significant influence on averaged saturated lipid content within algal cells of 2 taxa, pennate ribbon colonies ($p < 0.001$, Table 1), and *Attheya* spp. ($p < 0.001$), over the length of the study. *N. frigida* only showed a significantly different response ($p < 0.001$) when the last 2 data points (28 and 30 May) were removed, owing to a different lipid accumulation response, discussed below.

Plots of the average saturated lipid content of the 3 taxa revealed seasonally relevant and taxa-specific trends (Fig. 5), when using spectrochemical imaging analyses. Saturated lipid content was at the lowest level at the start of the study; for each identified

Table 1. Results of matched pair Student's *t*-test for taxa averaged lipid (CH_2+CH_3) and protein (Amide I) content, and lipid to protein ratio per cell between thick and thin snow covers, and overall averaged lipid, protein and ratio values for taxa under both snow covers. Bolded numbers identify significant p-values ($p < 0.05$); numbers within brackets denote sample size (n)

Parameters	*Nitzschia frigida*	Pennate ribbon colony	*Attheya* spp.
CH_2+CH_3			
p-value	0.063 (15)	**<0.001** (13)	**0.001** (14)
	0.001[a] (13)		
Thin avg.	1.3 (15)	1.5 (13)	0.69 (14)
Thick avg.	0.84 (15)	0.81 (15)	0.41 (14)
Amide I			
p-value	0.79 (15)	0.83 (13)	0.87 (14)
Thin avg.	1.1 (15)	1.9 (13)	0.80 (14)
Thick avg.	1.3 (15)	2.1 (15)	0.86 (14)
Ratio			
p-value	**0.0001** (15)	**<0.0001** (13)	**<0.0001** (14)
Thin avg.	1.2 (15)	0.79 (13)	0.89 (14)
Thick avg.	0.58 (15)	0.39 (15)	0.51 (14)

[a]p-value recalculated after removal of 28 and 30 May data points

taxon, the lipid content did not differ between snow covers, and was still very low in mid-March. Over the duration of the study, the averaged lipid content under thin snow cover tended to be greater than that under thick snow cover. In general, cells under thin snow cover responded to increasing light levels in an approximately linear fashion, while the response under thick snow cover was later and appeared to be exponential.

Under thin snow cover, between 21 April and 30 May, the lipid content of *N. frigida* (Fig. 5A) increased rapidly: the positive linear regression was significant ($p < 0.05$, $r^2 = 0.41$). Under thick snow cover, the lipid content remained low and almost unchanged until late May, when a rapid increase was observed. This was best modelled by an exponential curve that was significant ($p < 0.05$, $r^2 = 0.81$). Overall, *N. frigida* accumulated the greatest lipid content under both thin and thick snow covers.

Saturated lipid content of the pennate ribbon colonies (Fig. 5B) rapidly increased under thin snow cover over the first portion of the study (11 March to 1 May) and then remained relatively stable. Linear regression analysis for thin snow data was significant ($p < 0.01$, $r^2 = 0.48$). Cell lipid content under thick snow remained relatively low, increasing gradually during the second half of the study period. Saturated lipid content under thick snow cover did not exhibit any significant trend ($p > 0.05$, $r^2 = 0.36$), linear or exponential.

Averaged cell lipid content of *Attheya* spp. increased steadily between March and May (Fig. 5C). The trend under thin cover seemed to be linear, but the data were highly variable ($p > 0.05$, $r^2 = 0.21$). Lipid content under thick snow also increased, but at a much slower rate. Under thick snow, *Attheya* spp. did not show any markedly significant trends, whether fitted with a linear (data not shown) or an exponential curve ($p > 0.05$). The latter gave a better fit, and yielded a larger r^2 value (0.46). Importantly, *Attheya* spp. had the lowest lipid content of the 3 taxa examined (see 'Discussion').

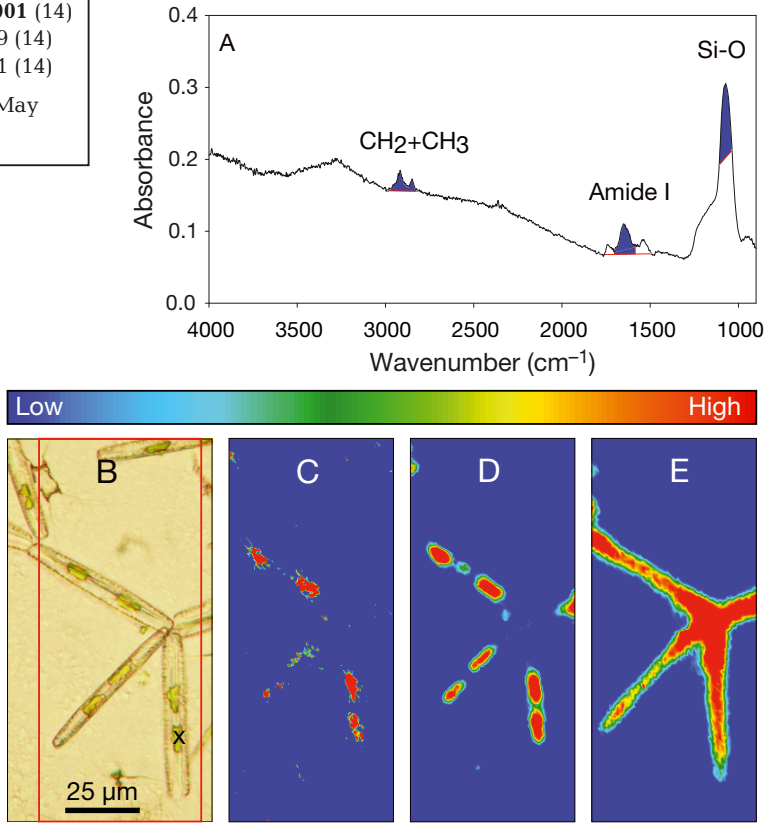

Fig. 4. FTIR spectrochemical image analysis of a *Nitzschia frigida* diatom colony, acquired as two 64 × 64 IR images, as a total of 8092 spectra. (A) Typical diatom FTIR spectrum acquired from chloroplast, showing band areas (shaded blue with red baselines) defined for saturated lipid (CH_2+CH_3), protein (Amide I) and silica (Si-O). (B) Light microscope image (40×) of the colony. The red rectangle outlines the FTIR imaged region and **x** shows the location of the spectrum in (A). False colour images illustrate the distribution of biomass, based on integrated band intensities (from 'high' to 'low', as shown in the colour scale bar) for: (C) lipid, (D) protein, and (E) silica

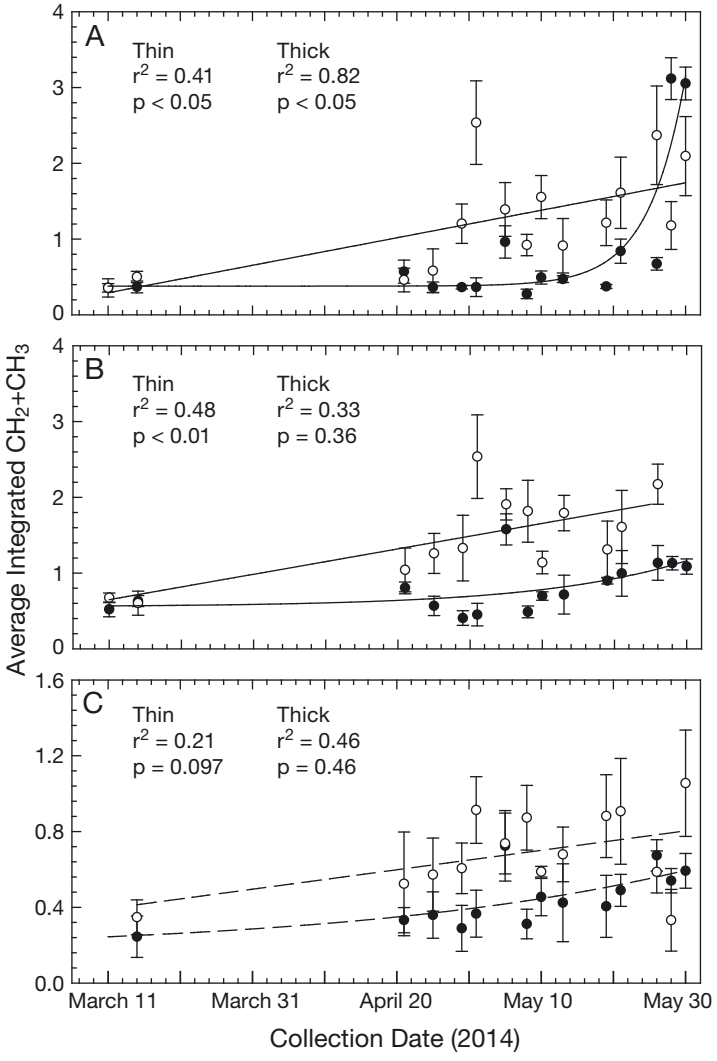

Fig. 5. Average (±SD) integrated saturated lipid (CH_2+CH_3) content per cell under (○) thin ($f = y_0 + a \cdot x$) and (●) thick ($f = y_0 + a \cdot e^{(b \cdot x)}$) snow cover sites for (A) *Nitzschia frigida*, (B) pennate ribbon colony and (C) *Attheya* spp., between 11 March and 30 May 2014. Solid lines represent significant regression fit at $p < 0.05$, whereas dashed lines are non-significant. Note: The data for all 3 taxa under thick snow cover showed an anomalous increase on May 5. Removal of this point rendered all 3 regressions significant, but results for the full data set are shown here

Protein

Averaged cell protein content for all diatom taxa (Fig. 6) did not follow any temporal linear trends, nor was snow thickness a significant influencing factor (Table 1, $p > 0.05$). However, there was a tendency for diatoms growing under thick snow to have slightly greater protein content as demonstrated by their period averaged content. Pennate ribbon colonies were found to contain the greatest averaged protein content per cell.

Saturated lipid to protein ratio

The saturated lipid to protein ratio (Fig. 7) closely followed the trends that were observed for cell lipid content alone (Fig. 5). However, the paired *t*-test revealed a greater significance between snow covers for the lipid to protein ratio: *N. frigida* ($p < 0.01$), pennate ribbon colonies ($p < 0.01$) and *Attheya* spp. ($p < 0.01$) (Table 1). The ratios were generally greater for cells under thin snow cover than those under thick. Compared to the other taxa, ratios were lowest on average for pennate ribbon colonies, reaching maximum values of 1.26 and 0.62 under thin and thick snow covers, respectively, compared to those of *N. frigida* (~2.0 for thin and thick) and *Attheya* spp. (~1.3 and 1.1) at the end of the study.

DISCUSSION

FTIR techniques have been used for bulk analysis of algal cells (Stehfest et al. 2005, Dean et al. 2010) and on cells from culture-based experiments (Heraud et al. 2008, Sackett et al. 2013, 2016). This study is the first to use FTIR spectrochemical imaging to monitor biomass composition in individual cells of specific diatom taxa, collected in the field over the course of an Arctic spring. Light transmission through sea ice is greatly dependent on the thickness of the snow cover and its attenuation of incoming solar radiation (Perovich et al. 1998). This inverse relationship controls the amount of light reaching the bottom ice algal community, and can significantly affect primary production and biomass accumulation, (for a review see Leu et al. 2015) as well as biomass composition through acclimation strategies (Palmisano et al. 1985, Mock & Kroon 2002b, Thomas & Diekmann 2002, Leu et al. 2006, Gradinger 2009, Campbell et al. 2016). As reported in a parallel study (Campbell 2015, Campbell et al. 2016), PAR transmittance through the sea ice increased during our study from 1.6 and 1.1% on 21 April to 4.4 and 3.2% by 30 May under thin and thick snow covers, respectively. The powerful technique of IR transmission imaging provided important information on the molecular changes that occurred within each diatom taxa (individual cell resolution) over the winter to spring transition, enabling a detailed autecological analysis of the influence of snow cover conditions on taxa-specific biomass composition.

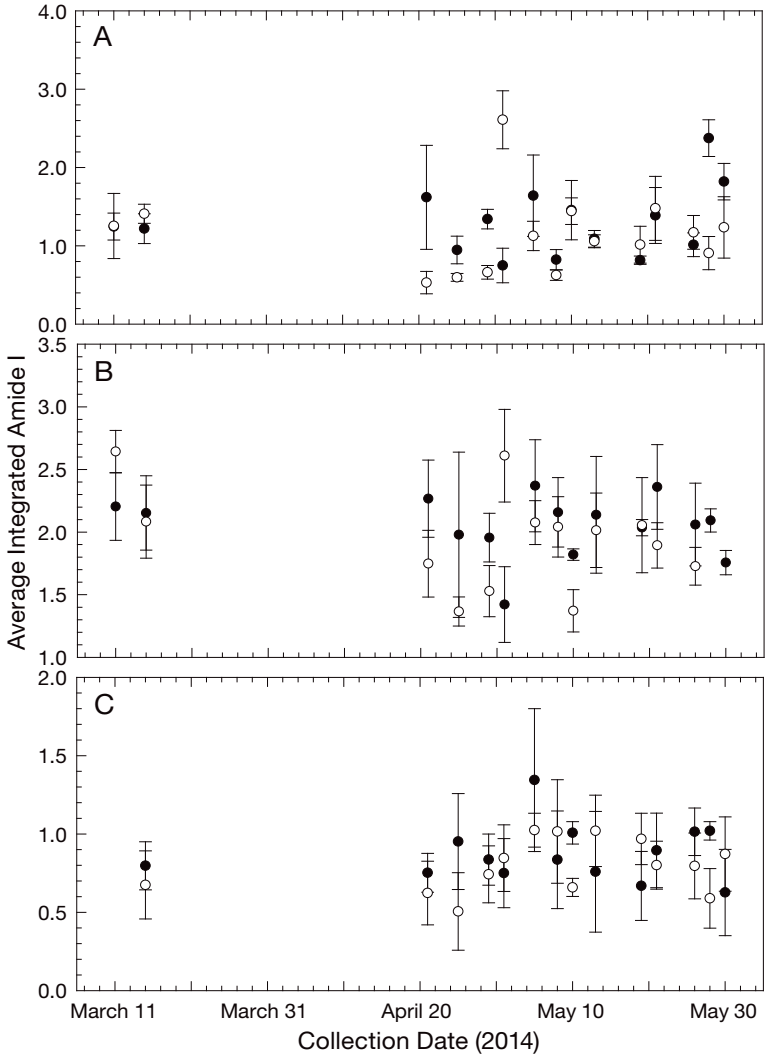

Fig. 6. Average (±SD) integrated protein (Amide I) content per cell under (○) thin ($f = y_0 + a \cdot x$) and (●) thick ($f = y_0 + a \cdot x$) snow cover sites for (A) *Nitzschia frigida*, (B) pennate ribbon colony, and (C) *Attheya* spp., between 11 March and 30 May 2014. Trends were non-significant and therefore not shown. The tested formulae are, however, given as the p-values are reported in Table 1

On the early sampling dates, 11 and 15 March, saturated lipid content was at its lowest level for all taxa, whether under thin or thick snow cover (Fig. 5). Comparable results were also seen in protein content and saturated lipid to protein ratio (Figs. 6 & 7, respectively). The model data shows that TOA shortwave irradiance was very low, <100 W m^{-2}, at this time (Fig. 3). Given that snow cover depths were significantly different, we conclude that all diatoms during this early period were in a state of shade-acclimation, associated with Phase I (pre-bloom, low insolation phase) of a generalized 3-phase bloom classification system (Leu et al. 2015).

By 21 April, the ice algal community had appeared to enter Phase II (bloom phase, increasing insolation, Leu et al. 2015) of their vernal bloom, as seen in Fig. 5. Gradual changes occurred over the next 4 wk (21 April to 19 May). Under thin snow cover, all taxa accumulated lipids linearly, while averaged lipid content in cells under thick snow cover remained comparable to that observed in Phase I.

All algae responded similarly, but the FTIR data showed that each taxa responded at a different rate, and that those rates differed with snow cover. Lipid content increased by about 50% over this time period in both *Nitzschia frigida* and pennate ribbon colonies. The increase in saturated lipid content for *Attheya* spp. was much slower, increasing by approximately 20% in the same time period. This steady accumulation of lipid can be interpreted in terms of an acclimation strategy that is transitioning away from light-limited conditions, benefitting from increased light to store high-energy biomass (Falkowski & LaRoche 1991). In contrast, lipid accumulation under thick snow cover was best modelled as an exponential increase, being initially very slow but transitioning to a more rapid rise later in the bloom.

At the end of the collection period, 21 May to 30 May, several events occurred simultaneously. Increasing temperatures led to melt onset and a rapid drop in albedo; a warm front accompanied by a heavy snowstorm occurred on 24 May, with light snow through to 26 May, briefly altering the snow cover. *N. frigida* exhibited the most dramatic response (during and after the snowstorm): lipid cell content rapidly increased under both thin and thick snow covers. For the latter, it increased exponentially to values that exceeded those under thin cover. The other taxa continued with a steady linear increase under thin snow, and slow exponential increase under thick. The varied responses in Fig. 5 were most likely dependent on additional factors such as nutrients, which we consider below (Mock & Kroon 2002a,b).

Cellular protein content (Fig. 6) did not change significantly during the course of the study, nor were there any significant differences between thin and thick snow covers. Among the taxa examined, pennate ribbon colonies contained the greatest averaged

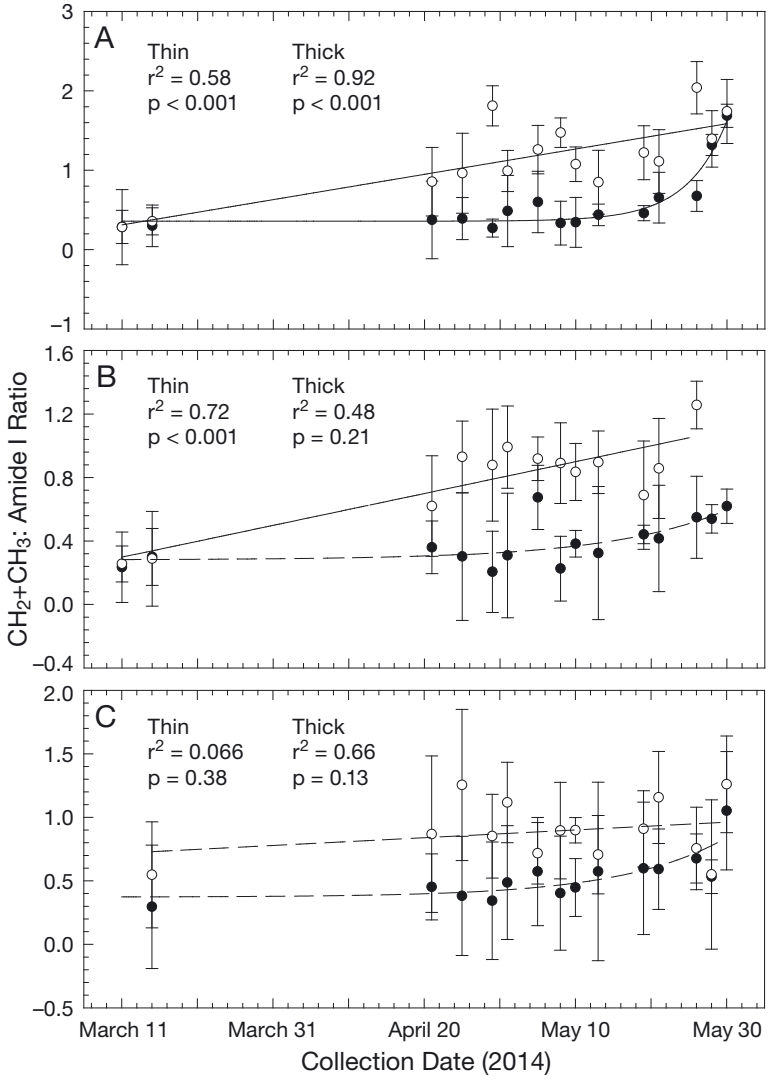

Fig. 7. Average (±SD) saturated lipid (CH_2+CH_3) to protein (Amide I) ratios per cell under (○) thin ($f = y_0 + a \cdot x$) and (●) thick ($f = y_0 + a \cdot e^{(b \cdot x)}$) snow cover sites for (A) *Nitzschia frigida*, (B) pennate ribbon colony, and (C) *Attheya* spp., between 11 March and 30 May 2014. Solid lines represent significant regression fit at $p < 0.05$, whereas dashed lines are non-significant

protein content per cell, while *Attheya* spp. contained the least. The interplay of different factors is implicated. Greater allocation of carbon to protein has been reported for low light conditions (Smith et al. 1987, Falkowski & LaRoche 1991). The occurrence of slightly greater protein content under thick snow cover has also been attributed to greater nutrient resource in the surrounding environment (Mock & Kroon 2002a). Under high light conditions, diatoms may have a greater photosynthetic carbon allocation to storage lipids than to membrane lipids, resulting in a reduction in chloroplast volume (Mock & Kroon 2002b, Leu et al. 2010). The overall concentrations of nitrogen under both snow covers were concluded to be co-limiting with light, over diel periods, during most of this (Campbell et al. 2016) and other (Lavoie et al. 2005) studies. Overall, the low, relatively stable levels of protein recorded through the FTIR analysis were concluded to be attributable to the combination of a relatively low-light, nutrient-deplete environment.

The variation in saturated lipid to protein ratio over the bloom was observed to be strongly lipid-driven (Fig. 7), in that the trends were very similar to those for saturated lipid content (Fig. 5). While cell protein content was fairly stable under both snow covers (Fig. 6), division of lipid content by protein content served to normalize some of the day-to-day, cell-to-cell variability. Consequently, the ratio provided a clearer distinction of the significant trends observed from lipid content alone. The ratios show that there was a clear preferential allocation of carbon towards lipid production throughout the study under the thin snow cover. The exponential increase under thick snow suggested this allocation towards lipid production mainly occurred near the end of our study period when light transmission to the ice algal layer was increasing, as was chlorophyll *a* concentration (see Campbell et al. 2016). An increase in the carbohydrate to protein ratio (Gosselin et al. 1990) and similarly an increase in POC to PON ratios (Campbell et al. 2016, Niemi & Michel 2015) were predictive of a transition from a light-limited to a nutrient-limited environment. Photosynthetic-driven carbon allocation has been reported to be redirected from protein (nitrogen rich) complexes to lipid structures within the cell, when nutrients become limiting near the end of Phase II of an algal bloom (Mock & Kroon 2002a, Smith et al. 1997, Stehfest et al. 2005). Thus, the significant increases in saturated lipid to protein ratio, dominated by changes in saturated lipids, were likely reflecting an increase in light, which led to increased production and greater nutrient demand and ultimately, greater nutrient-limitation.

To investigate nutrient dependence, saturated lipid content for each taxON was plotted against bottom-ice (bottommost 5 cm) bulk POC and nitrate plus nitrite ($NO_3 + NO_2$) data from a parallel related study (Campbell et al. 2016). All taxa demonstrated a sig-

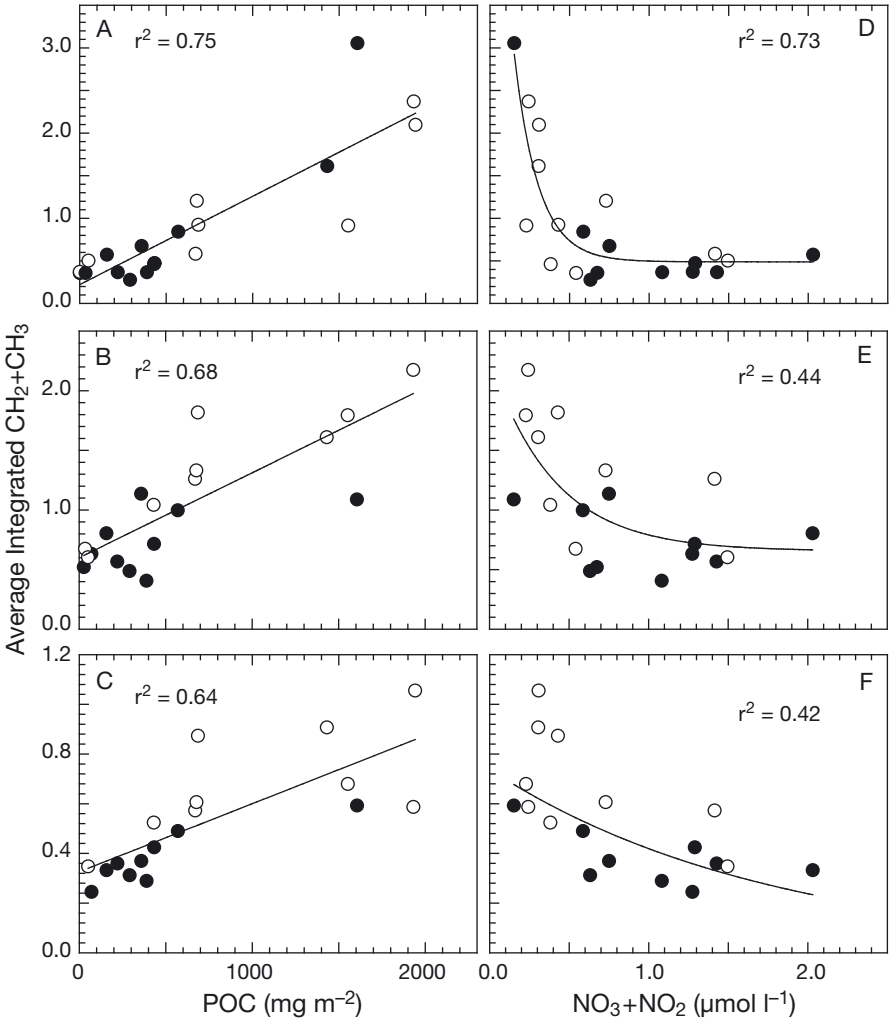

Fig. 8. Average (±SD) saturated lipid (CH_2+CH_3) versus (A–C) particulate organic carbon (POC) and (D–F) nitrate plus nitrite (NO_3+NO_2) under (○) thin and (●) thick snow cover sites for (A,D) *Nitzschia frigida*, (B,E) pennate ribbon colony, and (C,F) *Attheya* spp. Significant trend lines are plotted in the form $f = y_0 + a \cdot (1 - e^{(-b \cdot x)})$ for panels A–C, and $f = y_0 + a \cdot e^{(-b \cdot x)}$ for panels D–F

nificantly increased allocation of carbon to lipids as the ice algal community accumulated biomass, independent of snow cover (Fig. 8A–C). The opposite response was observed with [NO_3 + NO_2] concentrations; saturated lipid allocation significantly decreased with increased nutrient availability in the sea ice (Fig. 8D–F). These results confirm our interpretation that increased nutrient limitation had led to greater lipid allocation as the bloom progressed towards the end of the growth season.

Interestingly, our results suggest that smaller cells have a lower nutrient demand for growth, making more efficient use of scarce resources. Among the studied taxa, *N. frigida* exhibited the greatest sensitivity to changing conditions, followed by the pennate ribbon colonies and then the *Attheya* spp.. This order also represents a decreasing cell size. K. Campbell unpubl. data suggested that limiting nutrient availability in the region leads to dominance of smaller centric diatoms by the end of the ice algal bloom. Our taxa-specific results provide direct evidence to support this hypothesis, confirming the value of the FTIR imaging technique to autecological studies of algae.

CONCLUSIONS

This study revealed significant differences in the biomass composition of bottom ice diatoms between thin and thick snow covers, along with noticeable differences among algal taxa. The relative concentrations of cell-averaged saturated lipid and protein, determined through FTIR spectrochemical imaging,

were shown to be powerful proxies that enabled examination of individual diatom responses to light and nutrient limitation. Changes in lipid content highlighted a differing response between specific diatom taxa. An increase in carbon allocation to high-energy storage lipids coincided with increasing light and limited nutrient availability, experienced most strongly by larger diatoms that would have a greater biomass-based nutrient demand for growth. This spectroscopic study facilitates the autecological investigation of diatoms and stands to propel our understanding of community interactions of these important taxa in the Arctic marine food web. In the future, we will examine a broader range of algal species using this powerful technique both in the laboratory and, with portable models, in the field.

Acknowledgements. This work was supported by funding from the Natural Sciences and Engineering Research Council (NSERC) undergraduate research awards to N.M.P. and C.R.F., Northern Scientific Training Program awards to C.R.F. and K.C., NSERC operating grants to C.J.M., K.M.G., and J.K.E., and University of Manitoba Faculty of Science field work support program award to C.R.F. Polar Knowledge Canada is thanked for in-kind logistical support. Special thanks are extended to Alexandra Ciapala for assistance in developing the FTIR-diatom technique, to Aurelie Delaforge, Tim Papakyriakou, Sebastian Luque, Brent Else, and other ICE-CAMP participants for field support, and to the Ekaluktutiak Hunters and Trappers Organization and residents of Cambridge Bay, Nunavut for their support of the ICE-CAMPS field program. This is a contribution to the programs of MEOPAR, Arctic Science Partnership, and the Canada Excellence Research Chair unit at the Centre for Earth Observation Science. We are grateful to the 2 reviewers for insightful comments that improved the paper.

LITERATURE CITED

Campbell K (2015) Sea ice microbiology data - Cambridge Bay 2014. Polar Data Catalogue, Canadian Cryospheric Information Network, Winnipeg. www.polardata.ca/pdcsearch/PDCSearchDOI.jsp?doi_id=12165 (accessed 25 Nov 2016)

Campbell NA, Reece JB, Urray LA, Cain ML and others (2008) Biology, 8th edn. Pearson Education, San Francisco, CA

Campbell K, Mundy CJ, Landy JC, Delaforge A, Michel C, Rysgaard S (2016) Community dynamics of bottom-ice algae in Dease Strait of the Canadian Arctic. Prog Oceanogr 149:27–39

Cota GF, Smith RE (1991) Ecology of bottom ice algae: II. Dynamics, distributions and productivity. J Marine Syst 2:279–295

Dean AP, Sigee DC, Estrada B, Pittman JK (2010) Using FTIR spectroscopy for rapid determination of lipid accumulation in response to nitrogen limitation in freshwater microalgae. Bioresource Technol 101:4499–4507

Environment Canada (2016) Daily data report April 2014: Cambridge Bay. http://climate.weather.gc.ca/ (accessed 12 July 2016)

Falkowski PG, LaRoche J (1991) Acclimation to spectral irradiance in algae. J Phycol 27:8–14

Findlay CR, Wiens R, Rak M, Sedlmair J and others (2015) Rapid biodiagnostic ex-vivo imaging at 1 µm pixel resolution with thermal source FTIR FPA. Analyst 140: 2493–2503

Findlay CR, Morrison J, Mundy CJ, Sedlmair J, Hirschmugl CJ, Gough KM (2017) Thermal source Fourier Transform Infrared microtomography applied to Arctic sea ice diatoms. Analyst 142:660–669

Fortier M, Fortier L, Michel C, Legendre L (2002) Climatic and biological forcing of the vertical flux of biogenic particles under seasonal Arctic sea ice. Mar Ecol Prog Ser 225:1–16

Gosselin M, Legendre L, Therriault JC, Demers S (1990) Light and nutrient limitation of sea-ice microalgae (Hundson Bay, Canadian Arctic). J Phycol 26:220–232

Gradinger R (2009) Sea-ice algae: major contributors to primary production and algal biomass in the Chukchi and Beaufort Seas during May/June 2002. Deep Sea Res II 56:1201–1212

Griffiths P, de Haseth J (2007) Fourier transform infrared spectrometry, 2nd edn. Wiley Inter-Science, Hoboken, NJ

Heraud P, Stojkovic S, Beardall J, McNaughton D, Wood BR (2008) Intercolonial variability in macromolecular composition in P-starved and P-replete *Scenedesmus* populations revealed by infrared microspectroscopy. J Phycol 44:1335–1339

Kirst GO, Wiencke C (1995) Ecophysiology of polar algae. J Phycol 31:181–199

Lalli C, Parsons T (1997) Biological oceanography and introduction, 2nd edn. Elsevier Butterworth-Heinemann, Amsterdam

Lavoie D, Denman K, Michel C (2005) Modeling ice algal growth and decline in a seasonally ice-covered region of the Arctic (Resolute Passage, Canadian Archipelago). J Geophys Res 110:C11009

Legendre L, Ackley SF, Dieckmann GS, Guliksen B and others (1992) Ecology of sea ice biota. Polar Biol 12:429–444

Leu E, Wängberg SA, Wulff A, Falk-Peterson S and others (2006) Effects of changes in ambient PAR and UV radiation on the nutritional quality of an Arctic diatom (*Thalassiosira antarctica* var. *borealis*). J Exp Mar Biol Ecol 337:65–81

Leu E, Wiktor J, Søreide JE, Berge J, Falk-Petersen S (2010) Increased irradiance reduces food quality of sea ice algae. Mar Ecol Prog Ser 411:49–60

Leu E, Søreide JE, Hessen DO, Falk-Peterson S, Berge J (2011) Consequences of changing sea-ice cover for primary production and secondary producers in European Arctic shelf seas: timing, quantity, and quality. Prog Oceanogr 90:18–32

Leu E, Mundy CJ, Assmy P, Campbell K and others (2015) Arctic spring awakening-steering principles behind the phenology of vernal ice algae blooms. Prog Oceanogr 139:151–170

Markus T, Stroeve JC, Miller J (2009) Recent changes in Arctic sea ice melt onset, freezeup, and melt season length. J Geophys Res Oceans 114:C1204

Miller C, Wheeler P (2012) Biological oceanography, 2nd edn. John Wiley & Sons, Oxford

Mock T, Gradinger R (2000) Changes in photosynthetic carbon allocation in algal assemblages of Arctic sea ice with decreasing nutrient concentration and irradiance. Mar Ecol Prog Ser 202:1–11

Mock T, Kroon B (2002a) Photosynthetic energy conversion under extreme conditions—I: important role of lipids as structural modulators and energy sink under *N*-limited growth in Antarctic sea ice diatoms. Phytochemistry 61: 41–51

Mock T, Kroon B (2002b) Photosynthetic energy conversion under extreme conditions—II: the significant of lipids under light limited growth in Antarctic sea ice diatoms. Phytochemistry 61:53–60

Mundy CJ, Barber DG, Michel C (2005) Variability of snow and ice thermal, physical and optical properties pertinent to sea ice algae biomass during spring. J Marine Syst 58: 107–120

Niemi A, Michel C (2015) Temporal and spatial variability in sea-ice carbon. Elem Sci Anth 3:78

Niemi A, Michel C, Hille K, Poulin M (2011) Protist assemblages in winter sea ice: setting the stage for the spring ice algal bloom. Polar Biol 34:1803–1817

NREL (National Renewable Energy Laboratory) (2016) MIDC SOLPOS calculator. www.nrel.gov/midc/solpos/solpos.html (accessed 12 May 2016)

Palmisano AC, SooHoo JB, Sullivan CW (1985) Photosynthesis–irradiance relationship in sea ice microalgae from McMurdo Sound, Antarctica. J Phycol 21:341–346

Parkinson CL, Comiso JC (2013) On the 2012 record low Arctic sea ice cover: combined impact of preconditioning and an August storm. Geophys Res Lett 40: 1356–1361

Perovich DK, Roesler CS, Pegau WS (1998) Variability in Arctic sea ice optical properties. J Geophys Res Oceans 103:1193–1208

Poulin M, Daugbjerg N, Gradinger R, Ilyash L and others (2011) The pan-Arctic biodiversity of marine pelagic and sea-ice unicellular eukaryotes: a first-attempt assessment. Mar Biodivers 41:13–28

Różańska M, Gosselin M, Poulin M, Wiktor JM, Michel C (2009) Influence of environmental factors on the development of bloom ice protest communities during the winter-spring transition. Mar Ecol Prog Ser 386:43–59

Sackett O, Petrou K, Reedy B, De Grazia A and others (2013) Phenotypic plasticity of Southern Ocean diatoms: key to success in the sea ice habitat? PLOS ONE 8:e81/85

Sackett O, Petrou K, Reedy B, Hill R and others (2016) Snapshot prediction of carbon productivity, carbon and protein content in Southern Ocean diatom using FTIR spectroscopy. ISME J 10:416–426

Smith REH, Clement P, Cota GF, Li WK (1987) Intercellular photosynthate allocation and the control of Arctic marine ice algal production. J Phycol 23:124–132

Smith REH, Gosselin M, Taguchi S (1997) The influence of major inorganic nutrients on the growth and physiology of high arctic ice algae. J Marine Syst 11:63–70

Søreide JE, Leu EVA, Berge J, Graeve M (2010) Timing of blooms, algal food quality and *Calanus glacialis* reproduction and growth in a changing Arctic. Glob Change Biol 16:3154–3163

Stehfest K, Toepel J, Wilhelm C (2005) The application of micro-FTIR spectroscopy to analyse nutrient stress-related changes in biomass composition of phytoplankton algae. Plant Physiol Bioch 43:717–726

Stitt DM, Kastyak-Ibrahim MZ, Liao CR, Morrison J, Albensi BC, Gough KM (2012) Tissue acquisition and storage associated oxidation considerations for FTIR microspectroscopic imaging of polyunsaturated fatty acids. Vib Spectrosc 60:16–22

Stroeve JC, Serreze MC, Holland MM, Kay JE, Malanik J, Barrett AP (2012) The Arctic's rapidly shrinking sea ice cover: a research synthesis. Clim Change 110:1005–1027

Thomas DN, Diekmann GS (2002) Antarctic sea ice – a habitat for extremophiles. Science 295:641–644

Editorial responsibility: Steven Lohrenz, New Bedford, Massachusetts, USA

Submitted: July 29, 2016; Accepted: February 9, 2017
Proofs received from author(s): March 27, 2017